Learning Machine Identification of Ferromagnetic UXO Using Magnetometry

Article *in* IEEE Journal of Selected Topics in Applied Earth Observations and Remote Sensing · February 2015

DOI: 10.1109/JSTARS.2014.2362920

2 authors:

Matthew Bray
Colorado School of Mines
2 PUBLICATIONS **4** CITATIONS
SEE PROFILE

Curtis Link
Montana Tech of the University of Montana
54 PUBLICATIONS **189** CITATIONS
SEE PROFILE

Learning Machine Identification of Ferromagnetic UXO Using Magnetometry

Matthew P. Bray and Curtis A. Link, *Member, IEEE*

***Abstract*—The fundamental problem in applying geophysical mapping to locate unexploded ordnance (UXO) is distinguishing true UXO from non-UXO. Enhancing the accuracy of UXO detection has multiple benefits, especially in the areas of cost savings and safety. We investigated discrimination approaches using both magnetic field data and numerically modeled data. Libraries of total field magnetic (TFM) responses were calculated using finite element modeling for three UXO types found at a Montana National Guard training site. UXO model parameters were varied over ranges of azimuth, declination, and depth resulting in approximately 600 models per UXO type. The modeled responses of finite-element model (FEM) and actual TFM field data were then used as training data in discrimination and classification approaches comparing neural networks (NN), random forests (RF), and support vector machines (SVMs). The prediction targets in the training process comprised three classes: 1) binary [UXO or noninteresting object (NIO)]; 2) multiclass (UXO round type and NIO); and 3) classes derived from multiclass self-organizing feature map (SOFM) analysis. The multiclass SOFM targets generated from site-specific field data were found to be optimal for UXO discrimination. The best performing combination of class selection types using recentered data for UXO detection rates of 100% resulted in a false alarm rate (FAR) of 28%.**

***Index Terms*—Classification, finite-element model (FEM), magnetics, neural networks (NN), random forest (RF), support vector machine (SVM), unexploded ordnance (UXO).**

I. Introduction

UNEXPLODED ordnance (UXO) is an explosive that has failed to detonate as originally intended. They pose a significant public safety hazard throughout the world and many parts of the United States. Current detection methods have moderate success in the removal of all UXO on-site using either time-domain electromagnetics (TEM) and/or total field magnetics (TFM). Our study focuses on UXO discrimination with TFM. Although TEM methods typically have higher precision and discrimination accuracy compared with TFM, survey costs are higher and current TEM equipment has limited use in areas that are heavily vegetated or have extreme terrain.

Manuscript received April 08, 2014; revised August 02, 2014; accepted September 30, 2014. Date of publication October 30, 2014; date of current version February 09, 2015.

M. P. Bray was with the Geophysical Engineering Department, Montana Tech, Butte, MT 59701 USA. He is now with the Reservoir Characterization Project, Department of Geophysics, Colorado School of Mines, Golden, CO 80401 USA (e-mail: mabray@mymail.mines.edu).

C. A. Link was with the Geophysical Engineering Department, Montana Tech, Butte, MT 59701 USA. He is now the Director of Freshman Engineering, Montana Tech Butte, MT 59701 USA (e-mail: CLlink@mtech.edu).

Color versions of one or more of the figures in this paper are available online at http://ieeexplore.ieee.org.

Digital Object Identifier 10.1109/JSTARS.2014.2362920

TFM measures the strength of the earth's magnetic field in nanoTeslas (nT). Magnetic anomalies are detected by removing the earth's background magnetic field from the measured total field. UXO are typically detectible to an ordnance's maximum penetration depth for common soil types if background noise is minimal [1]. Typically, for TFM data analysis, static dipole model parameters are estimated using inversion, and a subset of parameters from the inverted model is used to guide a classifier [2]. Another common methodology is to define a detection threshold that utilizes theoretical models to calculate the least favorable orientation and worst possible offset of UXO from a magnetometer sensor [3]. Detection thresholds are calculated from peak analytic signal amplitudes compared with the signal-to-noise ratio of the data [3]. Although both methods have been successfully implemented, false alarm rates (FARs) can be high when UXO anomalies are similar to noninteresting object (NIO) anomalies.

Various studies have shown that supervised learning machine methods are capable of improving discrimination rates and lowering costs [4]–[6]. They have shown success in decreasing FARs between 20% and 30% (for 100% UXO detection) using learning machines trained with site-specific data. Optimal classifiers use site-specific data because geology, soil properties, and remanent magnetization can influence the learning machines [6]. However, acquiring site-specific UXO data can be costly and time consuming and is not typically done on a routine basis.

Typical magnetic forward modeling approaches generally use homogeneous prolate ellipsoids to approximate irregularly shaped objects such as UXO. Previous work has shown that prolate ellipsoid analytical dipole responses are similar to measured UXO responses [7], [8]. However, a recent study [9] shows that realistic, complex UXO shapes can produce more accurate model responses than simple prolate ellipsoids. Churchill *et al.* [9] focused on changes in volume and shape of three ferromagnetic UXO at various orientations and determined that shape and volume of the UXO can change the calculated dipole moment as much as 25%–50%. To investigate the effect of realistic finite element modeling of UXO for discrimination, we calculated a library of TFM responses using complex UXO model shapes. These calculated models in conjunction with measured site-specific NIO responses were used as training data in discrimination and classification tests using neural networks (NNs), random forests (RF), and support vector machines (SVMs). In our investigation, we examine the variability of discrimination results between site-specific measured and finite-element modeled (FEM) data. A study by Hart *et al.* showed that outputs from a physics-based modeler

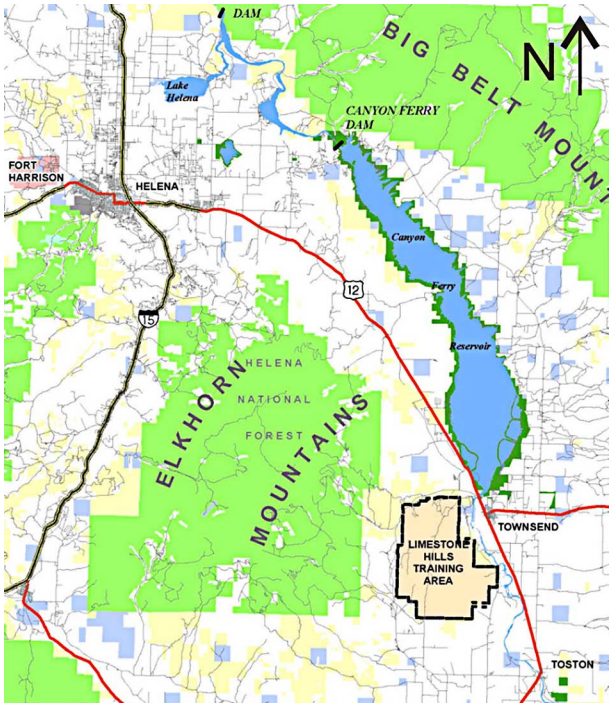

Fig. 1. Map of the Limestone Hills Training Area west of Townsend, MT, USA. Limestone Hills is an active live ammunition training area for the Montana Army Nation Guard. Approximately 454 acres were deemed at risk and have been cleared of UXO [12].

and site-specific NIO can have a good success rate for UXO discrimination [10].

To investigate the difference between measured and modeled data approaches, we implemented three different learning machines using a supervised methodology. Other studies have shown that learning machine performance can be site dependent [4], [11]. Thus, it becomes important to test the response of different learning machines before implementation. Supervised learning is desirable because it allows site-specific NIO data to be incorporated into the UXO discrimination process. The addition of NIO data is important when UXO and NIO have similar magnetic signatures [4]. Additionally, we examine how the centering of UXO data on the data collection grid affects prediction results. Selection of training data is critical to building an accurate learning machine. We investigated the training class selection process for 1) binary classification (UXO or NIO); 2) multiclass classification (UXO types and NIO); and 3) the use of unsupervised classification preconditioning for identifying class types. We applied our UXO classification processes to magnetic data collected from the Limestone Hills Training Area near Townsend, Montana.

The remainder of this paper is organized as follows. Section II discusses current learning machine methodologies, forward modeling, and discrimination methods; in Section III, specifications for FEM are discussed; Section IV gives an overview of NN, RF, and SVM, as well as the preprocessing of magnetic data; finally, we discuss applying our approach to the Limestone Hills Training Area data (Fig. 1).

II. UXO Discrimination

Previous UXO classification studies have focused on simple spheroid models. Hart *et al.* [10] used probabilistic NN (PNN) for three UXO contaminated sites to gauge the accuracy of binary (UXO/NIO) classifiers. The PNN inputs were physics-based point dipole model outputs for UXO and site-specific measured data for NIO. The study examined a wide array of model parameters and determined that depth, inclination, and UXO volume parameters resulted in the most accurate classifier. Their study also used measured UXO responses from the Buckley Field, CO site as the training set for discriminating UXO at The Badlands Bombing Range, SD. Interestingly, the training set was from a different geographic region and different round sizes were used for discrimination. Though FAR increased slightly, their results indicated that UXO discrimination problems might not be highly dependent upon geography. Multiclass PNN were also implemented to discriminate UXO types and NIO. This approach improved overall UXO discrimination, but increased FAR. The study concluded that two learning machines could be employed separately for binary discrimination and multiclass UXO classification.

In another UXO classification study, Zhang *et al.* [13] modeled homogeneous, metallic spheroids meant to resemble real UXO. These analytical models were used to generate training data by calculating the spheroidal mode coefficients for the metallic spheroids. Parameters varied were spheroid size, lateral position, rotational position, and declination. SVM and NN were implemented for classification of different shapes. The authors concluded that a large range of depths for UXO can significantly affect SVM accuracy and the addition of Gaussian noise to modeling results lowered prediction errors.

The selection of a representative training set is key for successful application of a supervised classification approach. Zhang *et al.* [6] developed an active learning algorithm to apply to sites where UXO dig costs are expensive and representative samples are difficult to obtain. Learning machines require representative samples for accurate classifications so the authors utilized the Fisher information matrix to iteratively build an optimal training set [6]. Over multiple iterations, a more representative training set is built. The authors used data from the Jefferson Proving Ground, IN, USA, which consisted of multiple UXO types ranging from mortars to projectiles and rockets. Active learning results improved receiver operating characteristic (ROC) curves by eliminating the large variances typical of random training set selection and also reduced the FAR.

Beran and Oldenburg [4] illustrated how bootstrap performance metrics can achieve results similar to active learning for PNN, SVM, and remanence threshold methods. Binary classification was used and the training set consisted of a generalized UXO class and a clutter class. A retrospective analysis was applied to TEM and TFM data from the Former Lowery Bombing and Gunnery Range, CO, USA, and Guthrie Road, MT. Retrospective analysis simulated how a training set can be improved as dig crews excavate targets of interest (TOIs). As digging progressed, targets classified as UXO were added to the training set. FAR and area under the curve rates were calculated

as digging information was added to the database. As training progressed using this approach, SVM outperformed both remanence and PNN in the early stages of training, but over time, remanence became the optimum classifier. The authors concluded that FAR are more sensitive to TOI that are difficult to identify.

Beran *et al.* [14] investigated criteria analysis to determine the distribution of TOI and identify unique target classes for developing optimal training sets. The authors analyzed multiple datasets with varying levels of data quality and implemented a hybrid selection process for the development of a training data set using supervised and unsupervised TOI selection. For supervised selection, TOI were manually identified when polarizabilities were similar to responses of known test items. Unsupervised selection was performed by analyzing the misfit of log-transformed polarizabilities with all items within the test set. The final training set was built by comparing supervised and unsupervised TOI selections and building a training set with the largest overlap between UXO and NIO. The novel target classes created improved overall classification by determining the total distribution of TOI.

III. Finite Element Forward Modeling

Forward modeling of UXO has typically utilized simple, prolate spheroid models. Churchill *et al.* [9] used three different UXO types modeled as three different shapes: 1) ellipsoid; 2) simple; and 3) complex to calculate dipole moments using an FEM approach. Depth and orientation values were based on ground truth data from a site in Montana. Volume differences among the three different shapes were small, but the calculated dipole moments of the shapes varied significantly. Hollow and solid shape dipole moments were also examined. Analytical solutions have shown that the dipole moment is a function of volume [15]. Altshuler [7] found that hollow and solid prolate spheroid analytical solutions have small differences in total induced magnetization. Churchill *et al.* [9] compared dipole magnitude differences for hollow and solid models using both COMSOL and UXOLab. The volume difference between hollow and solid models was caused by the change in casing thickness such that the volume of steel was reduced by 78% from solid to hollow complex ordnance. The modeled dipole moments for both the hollow and solid models for each shape showed little difference in magnitude. For all three ordnance types, hollow and solid models showed an average difference in dipole magnitude of 9%. Overall, the differences between hollow and solid models were determined to be insignificant when compared with background or sensor noise. Sanchez [16] also showed that significant volume reduction for an analytical model resulted in small differences in dipole response. Therefore, it appears that the dipole response is more strongly dependent on the shape of a UXO than its volume [9]. Modeled results were compared with dipole responses from validation data and results showed that complex shape models had a greater effect on the magnitude of the dipole moment than simple model shapes [9]. Results for all three UXO round types demonstrated that modeling using complex shapes has the potential to improve discrimination of UXO for TFM.

However, studies have shown that electromagnetic induction sensors can distinguish between hollow and solid ordnance. Shubitidze *et al.* [17] examined the effects of orientation, sharp points, and edges and finite wall thickness in hollow bodies and complex shapes. They were interested in magneto-quasistatic phenomena in electromagnetics and used the method of auxiliary sources as a simulation algorithm. They determined that using both the in-phase and quadrature components, they could detect differences between hollow and solid ordnance. For example, results indicated that the higher frequency half of the in-phase response contains information about the wall thickness of an ordnance. In addition, Chilaka *et al.* [18] used an electromagnetic induction system with extremely low frequencies to improve discrimination by a factor of 1.5. The expanded frequency range enabled discrimination between thin and thick-walled ferrous cylinders, which were indistinguishable in the typical electromagnetic induction band.

We used COMSOL Multiphysics version 4.2 finite element modeling to generate a library of TFM responses to be used for training sets in machine learning. Depth (cm) was measured from the center of mass of the UXO. Orientation of the UXO, dip (θ), and azimuth (Φ) uses a north–south alignment of the semimajor axis of the UXO; additionally, dip rotates toward the north-facing nose of the UXO. A negative dip rotates the nose down. Azimuth is positive clockwise around the z-axis [19].

Modeling did not take into account remanent magnetization because shock demagnetization typically occurs after rounds have been fired. Altshuler [7] showed low remanent magnetization of UXO as a result of shock demagnetization. Rounds found at Montana UXO sites often have little or moderate remanent magnetization [20]. UXO models are solid and assumed to be homogeneous with a relative permeability of 4000. UXO are typically made of steel and susceptibility can range from a few hundred to a few thousand; the magnetization saturates at values over 100 and increasing susceptibility produces only small variations in the response of the UXO [7]. For modeling UXO at Montana Limestone Hills, magnetic flux density was set to $\mathrm{Bx} = 3669.93$ nT, $\mathrm{By} = 20809.9$ nT, and $\mathrm{Bz} = -45315.4$ nT, corresponding to a magnetic inclination of 65°, declination of 10°, and magnetic strength of 50 000 nT [9].

IV. Learning Machines

Supervised learning machines have proven to be effective tools for nonlinear pattern recognition [4], [6], [10], [13]. Three different learning machines were implemented to demonstrate the large variances that may occur between learning machines for UXO classification. A comprehensive comparison of learning machines is necessary before field implementation in order to monitor performance at UXO sites as emphasized by Billings and Youmans [4], [21]. In general, learning machines use a set of training data where subsets x_i and y_i comprise the training set. A subset of model parameters that spans the feature space is selected, and a decision rule is formulated to correctly map x_i into y_i [22]. Additionally, a subset of the training data is withheld from the learning machine for evaluation (validation set) and testing (test set) purposes. We attempt to generate a learning

machine that has low-bias and low-variance. Low-bias indicates a learning machine might correctly map a test set; whereas, low-variance means the learning machine trained with different training sets, correctly maps a test set. For validation purposes for each learning machine, we use random subsampling 10-fold nested loop cross-validation [23]. Cross-validation chooses different subsets from the training set and averages the validation errors to determine an approximate error for a trained learning machine. Nested loop cross-validation varies the parameters of each learning machine to find the optimum parameters for each training set [24]. Training set sizes, or the quantity of UXO and NIO in a training set, were iteratively varied to find the optimum training set size using cross-validation. For training and validation, the best results occurred with 220 inputs (110 UXO and 110 NIO), of which 70% were used for training and 30% were used for validation. The test set was not involved in the training and validation process.

A. NNs

NN consist of computational neurons modeled after biological neurons, which have the properties of automatic learning, adaptation, organization, and the capability to solve nonlinear problems. NN have been successfully applied to multiple UXO cases for discrimination. Beran and Oldenburg [4] used PNN with bootstrap performance metrics to reduce FAR. Additionally, Zhang *et al.* [13] implemented NN to predict model parameters as a possible UXO discrimination method. NN are generally organized into input, hidden, and output layers. For further details about NN and the training process, refer to [25].

We used MATLAB's NN toolbox to implement a pattern recognition NN consisting of an input layer, three-hidden-layers, and one output layer. The number of hidden layers, the number of neurons, and the type of transfer functions were iteratively varied to find the optimum configuration. The optimization process tested up to 30 neurons in the first hidden layer, 25 neurons in the second hidden layer, and 20 neurons in the third hidden layer. Though two layer networks should be able to approximate any arbitrary decision boundary, we found that three hidden layers were optimum for our problem [25]. The final best performing network configuration had hidden layers containing 25, 10, and 4 neurons in each layer. A scaled conjugate gradient training algorithm was used for training and was determined to produce the best results. Input data were scaled from -1 to 1 and randomly split into training (70%) and validation (30%) sets. The test set was not involved in the training and validation of the NN. Random weights and biases were used for initialization with values between -1 and 1. All neuron transfer functions were tan-sigmoid.

B. SVM

SVM is a popular learning machine design that maps an input vector x_i into n-dimensional space by calculating the optimal hyperplane that separates two classes. After a hyperplane has been calculated, a trained SVM determines which side of the hyperplane characterizes a specific class [13], [26], [27]. UXO binary discrimination typically is suitable because of the differences in dipole moments between clutter and UXO. For UXO binary discrimination, nonlinear boundaries between clusters are expected. To account for UXO nonlinearity, a nonlinear kernel function is implemented, specifically a polynomial kernel. A grid search methodology is implemented during cross-validation to find the optimum free parameters for the SVM. The grid search accounted for the degree of the polynomial kernel, the regularization parameter C, and the ridge regularization parameter λ. Optimum parameters were selected from the best-performing configuration.

Multiclass SVM employs multiple binary SVM to separate k-classes. Two common multiclass SVMs are the one-against-one and the one-against-all. In the one-against-one approach, a collection of binary SVM calculates $\frac{k(k-1)}{2}$ hyperplanes that separate classes from each other [27]. A majority voting scheme is applied to determine the most likely class for an input vector. For the one-against-all approach, k classifiers are constructed for each class. For each classifier, a hyperplane is calculated between a class and $k-1$ other classes [27]. Final classification is determined by a majority voting scheme. Previous SVM UXO studies have focused upon the binary SVM application, i.e., one NIO and one UXO class [4], [6]. Our work utilizes the binary and one-against-one approach for multiclassification. An iterative one-against-one approach produced lower FAR than the one-against-all approach. We utilized freely distributed software called SVM and Kernel Methods MATLAB Toolbox [26], [28]. The one-against-one-approach used a polynomial kernel function for classification.

C. Random Forests

RF represent a classification or regression method that uses an ensemble of decision trees [29]. A decision tree is built using a bootstrap sample of the training data [30]. Bootstrap aggregation (bagging) and random variable selection generate decision trees that have low correlation to each other and an ensemble of unpruned trees is used to reduce prediction variance. Bagging generates multiple versions of a predictor by multiple bootstrap samples [31]. Each decision tree is unpruned or fully grown, which generates a low-bias classifier. RF averages over all decision trees that individually are low-biased and high-variance, but averaged over an ensemble of trees, generate both low-bias and low-variance classifiers [29], [32]. At nodes or decision locations on trees, a randomly chosen subset of predictors is used to maintain prediction strength, while allowing diversity among trees and maintaining low bias [29]. Use of RF for UXO discrimination or classification has not previously been reported in UXO literature, but has been used in microarray research [30], [31]. We used freely distributed RF MATLAB code based on Breiman's [29] original Fortran code and the R package randomForest [34], [35]. RF adjustable parameters were varied using a grid search methodology during cross-validation. The free parameters are the number of trees grown for the forest (*ntree*), the number of variables used at each split (*mtry*), and the minimal size of a terminal node of a decision tree (*nodesize*) [34]. We chose our optimum parameters based on the best-performing configuration.

V. Limestone Hills Training Area, MT, USA

A. Background

Beginning in 1958, the Montana Army National Guard began using the Limestone Hills for live-fire training with a variety of munitions. In 1993, the U.S. Army Corps of Engineers concluded that Limestone Hills was a public safety risk and the Bureau of Land Management closed 8000 acres of public land. The munitions response site comprises approximately 454 acres within the area of risk and the site has now been cleared of UXO.

B. Validation Database

Validation (ground truth) data were recorded along with TFM response data from a 2005 survey conducted by Geolex Inc. and Sky Research at Limestone Hills. The survey collected data from 233 grids $25\ \text{m} \times 25\ \text{m}$. TFM data were collected using a man-portable magnetometer array consisting of four Geometrics G-823 optically pumped cesium vapor magnetometers spaced 0.5 m apart maintained at a 0.5 m target sensor elevation. A magnetometer measures the strength of the earth's magnetic field in nanoTeslas (nT). The G-823 magnetometer has a cycle rate of 10 Hz [21]. Man-portable magnetometer arrays were selected because of the steep topography and presence of only ferrous UXO. Steep topography and vegetation caused magnetometer heights to vary up to ± 0.2 m from the specified 0.5 m height. A validation database was created to record ground truth information for each anomaly by validation crews, which resulted in a database containing x, y location, burial depth (d), orientation dip (θ) azimuth (θ), and UXO type. Churchill *et al.* [9] used the Limestone Hills database for the analysis of complex shapes for UXO FEM modeling.

UXOLab version 1.1.15 (University of British Columbia) was used to process and analyze the TFM data. TOIs were manually selected and analyzed using the UXOLab inversion module. UXOLab's inversion calculated dipole moment (Am^2), remanence (%), dipole azimuth, and dipole dip. The inversion results were also used to predict round size, depth, and orientation. The inversion results were added to the validation database along with the recorded ground truth information. For a detailed description of UXOLab, refer to [20] and [21]. The Limestone Hills validation database contains 1325 TOI of which 262 TOI were determined to be live, emplaced, or expended UXO. Emplaced ordnance was not included in this study because of different magnetic signatures caused by remanent magnetization [9], [36]. The validated database contained 1063 NIOs ranging from geologic anomalies to ferrous shrapnel and/or clutter. TOIs were excluded from this study if a mask of 2.5×2.5 m could not be generated for a centered magnetic anomaly. The final training set contained 220 UXO anomalies consisting of 76 mm, 90 mm, and 4.2 in illumination mortar rounds and 843 NIO anomalies. Magnetic data were gridded at 0.125 m (1/4 line spacing), which resulted in 441 pixels per anomaly that were used as inputs to the learning machines.

C. Anomaly Centering

The ability of learning machines to generate a decision boundary within a feature space is dependent upon input data patterns and relationships. Shifts or variances in anomaly locations can increase learning machine prediction error for training and evaluation. Previous work has utilized Euler deconvolution and continuous wavelet transforms for automatic detection of UXO anomaly centers (x_0, y_0, z_0) [37], [38], but such techniques have not been addressed in UXO-supervised learning literature. By utilizing a calculated geometric center for anomalies, human processing errors might be eliminated and a learning machine might have a greater chance of discriminating between UXO cluster types. The adjustment of TFM anomaly centers was an automated process that began with previous user chosen centers (using a GUI interface in UXOLab). TFM anomalies from the Limestone Hills training area were handpicked by experienced UXO processors for interpretation and inversion. Handpicked anomalies are henceforth referred to as noncentered anomalies. To adjust the center location of previously picked and validated anomalies, TFM anomaly centers $B(x_0, y_0)$ were automatically adjusted to the global minimum of the horizontal gradient of the magnetic anomaly assuming a constant elevation above the ground (Fig. 2). To validate our centering approach based on gradient centering, we performed classification to predict UXO type using centered and uncentered anomalies. FEM generated anomalies with known center locations were used for training (70%), validation (15%), and testing (15%). The first FEM simulation used anomalies centered directly above the center of the modeled UXO object; whereas, the second FEM simulation used FEM anomalies centered on the global minimum of the horizontal gradient of the anomaly. Anomalies centered directly above the UXO had a classification error of 2.0%, and anomalies centered using the gradient method had a classification error of 6.5%. Although noncentered results were more accurate by 4.5%, later application of gradient centering proved successful at decreasing FAR for real UXO anomalies.

D. Self-Organizing Feature Maps

Successful implementation of learning machines requires a statistically representative training set. For binary UXO discrimination (i.e., UXO/non-UXO), UXOs typically have large dipole moments at small angles, and NIOs have small dipole moments at large angles. Thus, binary classification is a reasonable goal [4]. However, UXO and NIO signatures overlap, which make representative training sets difficult to generate as binary classes. To develop a more objective way of selecting UXO and NIO classes for later supervised classification techniques, self-organizing feature maps (SOFMs) were implemented. SOFMs, or unsupervised NNs, use competitive learning, a method where each output neuron competes among other neurons to be activated, such that only one neuron (the winning neuron) is activated at a time [39], [40]. The SOFM begins by initializing random weights. The weight vector of the winning neuron or best matching unit (BMU) is selected by the Euclidian distance

$$\|x - m_c\| = \min\{\|x - m_i\|\} \tag{1}$$

where x is the input vector, m_i is the weight vector, and m_c is the weight vector closest to x. After the initial weights are

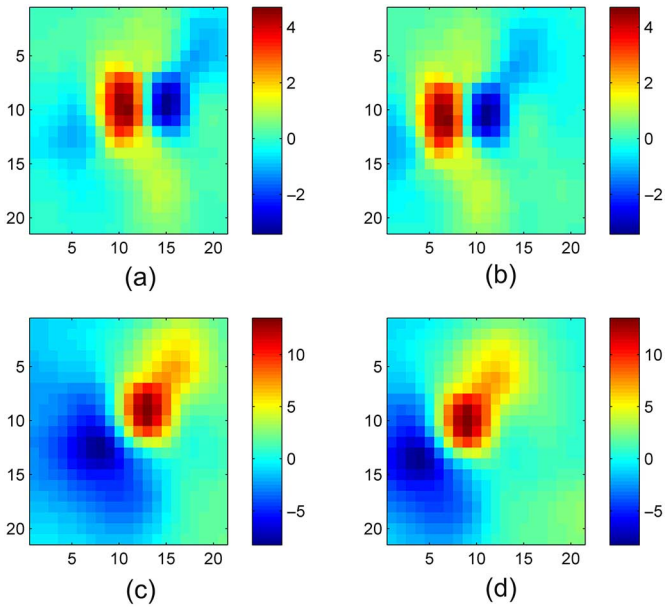

Fig. 2. Validated TFM anomaly of a 76-mm projectile from Limestone Hills. Magnetic units are in nT for TFM and $\frac{nT}{dx}$ for the horizontal gradient of TFM. (a) The gradient of the TFM of a noncentered UXO anomaly. (b) The gradient of the TFM of a centered UXO anomaly. (c) The TFM of the noncentered UXO anomaly. (d) The TFM of the centered UXO anomaly.

calculated, the winning neuron's weight vector moves a specified amount toward the current input vector. The updated weight is then

$$m_i(t+1) = m_i(t) + \alpha(t) h_{c(x),i} \left[x(t) - m_i(t) \right] \tag{2}$$

where t is the epoch, $x(t)$ is a sample of x, and the learning rate is $0 < \alpha < 1$, which decreases monotonically with each epoch. The neighborhood function is given by

$$h_{c(x),i} = \exp\left(-\frac{\|r_i - {r_c}^2\|}{2\sigma^2(t)} \right) \tag{3}$$

where r_i and r_c are the positions of neurons c and i, and $\sigma(t)$ is the width of the neighborhood function [39]. The operation is similar to learning in the human brain. When a biological neuron is activated, the surrounding neurons have more interaction with the firing neuron than neurons farther away [39].

Implementation of the SOFM was done with MATLAB's NN toolbox that uses Kohonen's algorithm [39]. Input data were scaled between -1 and 1. An SOFM was used to split UXO into two classes with large moments positioned at small angles and small moments positioned at large angles. The same methodology was implemented for NIO. UXO and NIO were grouped separately to avoid SOFM misclassification.

VI. Learning Machine Performance

We used the Limestone Hills validation database to examine the variability between FEM and site-specific training sets. Additionally, we investigated the FAR variability for different class types such as binary, UXO round labels, SOFM preclassification labels, and UXO round classification with either UXO FEM or site-specific data. For each class type, we compare the discrimination performance from three different learning machines: 1) NN; 2) SVM; and 3) RF.

TABLE I
Binary Results for Learning Machines 100% Confidence Level

Learning machine	Noncentered FAR (%)	Centered FAR (%)	FEM FAR (%)
NN	100	51	100
SVM	100	69	100
RF	71	49	100

A. Binary Classification

For binary classification, UXO anomalies (76 mm, 90 mm, and 4.2 in) comprise one class and all NIO anomalies represent a second class. Binary classification for UXO discrimination is typical because ordnance and clutter usually have large and small dipole moments at small and large angles, respectively [4]. We used three different simulations for binary classification: 1) training with measured noncentered measured anomalies; 2) measured gradient centered measured anomalies; and 3) FEM anomalies. All three simulations used site-specific NIO anomalies. FEM NIO responses were not generated because of the wide variety of objects comprising NIO. For each simulation, a training set was created from the Limestone Hills validation database by randomly selecting 110 vectors for each class type and applying nested loop cross-validation. The test set for FEM training had 953 anomalies (220 FEM UXO and 733 measured NIO) and the site-specific testing set had 843 anomalies (110 measured UXO and 733 measured NIO), respectively. Results for each learning machine are shown as ROC curves (Figs. 3 and 4). At the 100% confidence level (likelihood ratio), the noncentered anomalies resulted in high FAR for all learning machines (Table I), whereas the gradient-centered anomalies resulted in lower FAR. Furthermore, noncentered ROC curves vary for each learning machine, whereas gradient-centered anomalies result in ROC curves more similar to each other. Training with FEM anomalies (centered) and measured NIO resulted in ROC curves worse than noncentered results for all learning machines. Overall, the best simulation occurred with gradient-centered binary anomalies trained with RF, which had a FAR of approximately 49%. For all UXO to be dug at RF FAR of 49%, 355 of 723 NIO would be excavated, resulting in a decrease of 159 NIO from noncentered RF FAR.

B. UXO Round Types

Classifying different UXO round types can be important to UXO dig teams during the remediation effort. A class selection process based upon UXO round type and clutter has previously been shown to increase accuracy of UXO prediction but also might increase FAR [10]. For the Limestone Hills dataset, a training set was created by randomly selecting 36 anomalies for each class type (76 mm, 90 mm, 4.2 in and clutter) to which we applied nested loop cross validation. Targets and predictions were reduced to binary labels to produce an ROC curve for each

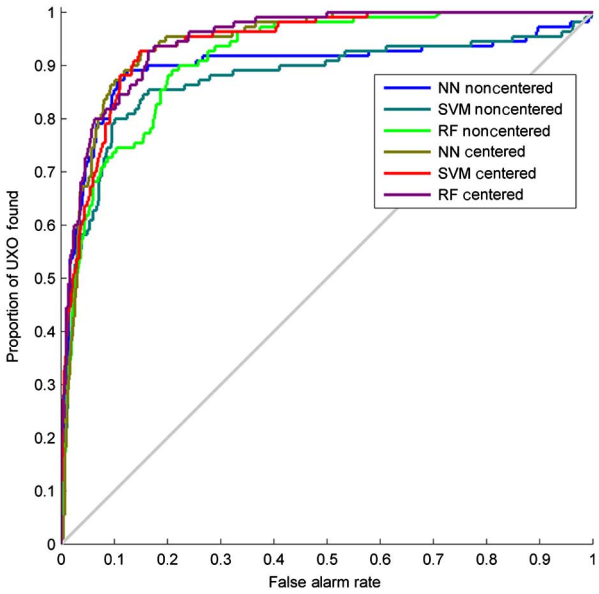

Fig. 3. ROC curves for the binary results of the noncentered and centered anomalies using NN, SVM, and RF.

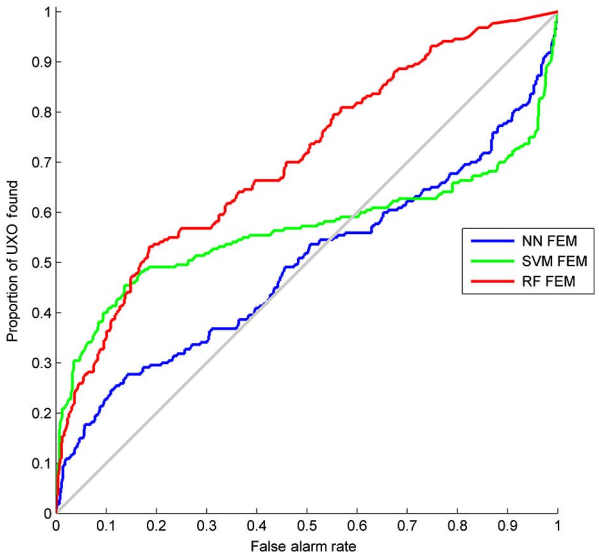

Fig. 4. ROC curves for the FEM-trained binary results using NN, SVM, and RF.

TABLE II
UXO TYPE RESULTS FOR LEARNING MACHINES

Learning machine	Confidence level	Centered FAR (%)	FEM FAR (%)
NN	90	19	96
NN	100	89	100
SVM	90	50	70
SVM	100	95	100
RF	90	58	70
RF	100	48	100

learning machine. Binary labels were calculated by summing all UXO classes into a merged UXO class, and then generating a merged ROC curve (Fig. 5) [4]. Classification using UXO round-type classes increased FAR for all three learning machines (Table II).

Training with UXO round types also allow the prediction of specific ordinance. UXO classification accuracy (RF) for

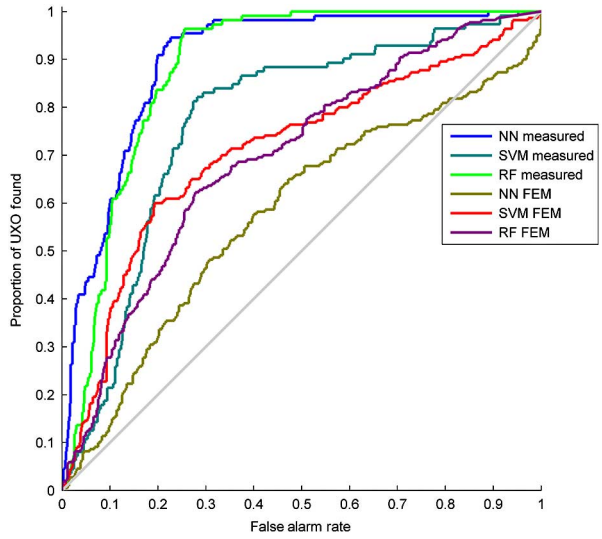

Fig. 5. ROC curves for the UXO round label results using NN, SVM, and RF. Learning machines were trained with FEM and measured anomalies.

76 mm, 90 mm, and 4.2 in illumination round were 50%, 48%, and 60%, respectively. Training with FEM round types with true NIO (36 vectors per class) resulted in ROC curves worse than noncentered results for all learning machines. Though results were poor, the UXO round type FEM classes performed better than binary FEM class.

C. UXO Type Classification Without NIO

Failure of UXO round types to decrease FAR from binary classes and predict specific ordinance type illustrates the problem of joint magnetic UXO discrimination and classification. In order to classify UXO types and maintain low FAR, we implement a separate learning machine that only classifies UXO type (i.e., no clutter or NIO in training). For implementation, learning machines were trained with FEM and measured anomalies to predict round type. The training set for measured data used 36 random vectors for each round type, while the training set for FEM data used approximately 600 vectors for each class type. Nested loop cross-validation was applied with each learning machine. Classification results for both FEM and measured anomalies were poor using this approach (Fig. 6).

Learning machines had low classification error (6.5%) when FEM data were used for training, validation, and testing. The low FEM classification error implies UXO classification is possible. Although FEM validation error was 8%, the validation error for measured anomalies was 42%. Differences between FEM and measured results might be caused by error in sensor height for measured data and possibly geologic effects at Limestone Hills. Limestone Hills UXO generally has little or no remanent magnetization, and we believe all UXO modeling parameters have been accounted for. Validation error from FEM results indicates two learning machines, one for discrimination and one for classification would provide the lowest FAR and accurate classification of UXO rounds. Limestone Hills data were originally interpreted with UXOLab's inversion for discrimination and classification. Using the three UXO

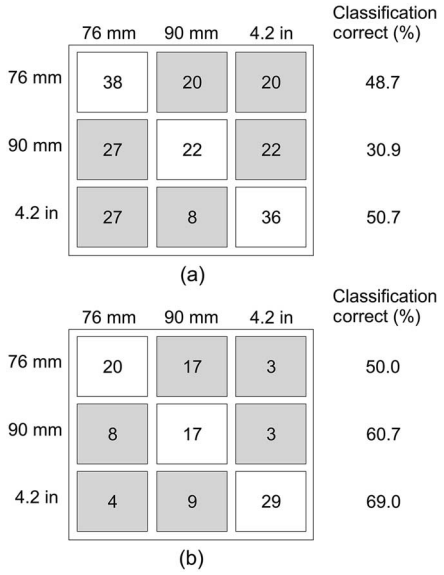

Fig. 6. Confusion matrix of classification results for only UXO anomalies. (a) RF trained with our FEM library and predicted three UXO rounds from the Limestone Hills validation database (76 mm, 90 mm, and 4.2 in illumination round). (b) RF trained with measured UXO anomalies and predicted three UXO rounds (76 mm, 90 mm, and 4.2 in illumination round).

TABLE III
CLASSIFICATION RESULTS FOR LEARNING MACHINES AND UXOLAB

Classification technique	76 mm accuracy (%)	90 mm accuracy (%)	4.2 in. accuracy (%)
NN measured	28.2	44.1	35.1
NN FEM	52.6	22.5	29.8
SVM measured	82.4	32.5	55.6
SVM FEM	25.6	42.3	69.0
RF measured	50.0	60.7	69.0
RF FEM	48.7	30.9	50.7
UXOLab	51.0	25.0	28.0

classification methods investigated in this study: 1) measured; 2) FEM; and 3) UXOLab, we were unable to achieve good classification results (Table III). Overall, classification results are better for learning machine FEM and learning machine measured anomalies than UXOLab by 9.5% and 25.9%, respectively.

D. SOFM Preclassification Labels

The higher FAR for UXO-type classification suggests that classes should be separated on anomaly differences (SOFM splits) instead of UXO type. For SOFM classification, significant overlap between UXO and NIO, in moment and angle space (Fig. 7), forces us to select multiple classes for UXO and NIO based upon anomaly variations. Using SOFMs, the UXO and NIO each split into two classes representing UXO and NIO with large and small dipole moments at small and large angles, respectively. A training set was created by randomly selecting 110 vectors from SOFM UXO classes. The quantity of each SOFM class selected was based upon the class population size. The same process was used for NIO. ROCs were generated for each learning machine and UXO and NIO classes were merged to generate binary labels for the test set (Fig. 8). FAR decreased for each learning machine when SOFM preclassification labels

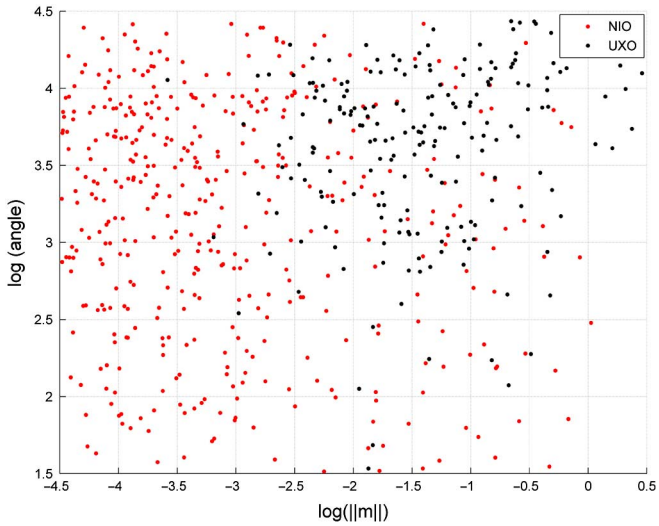

Fig. 7. Calculated moments and angles for the Limestone Hills validation database. Red circles represent NIO and black circles represent UXO. Significant overlap shows how the Limestone Hills dataset is not a binary problem.

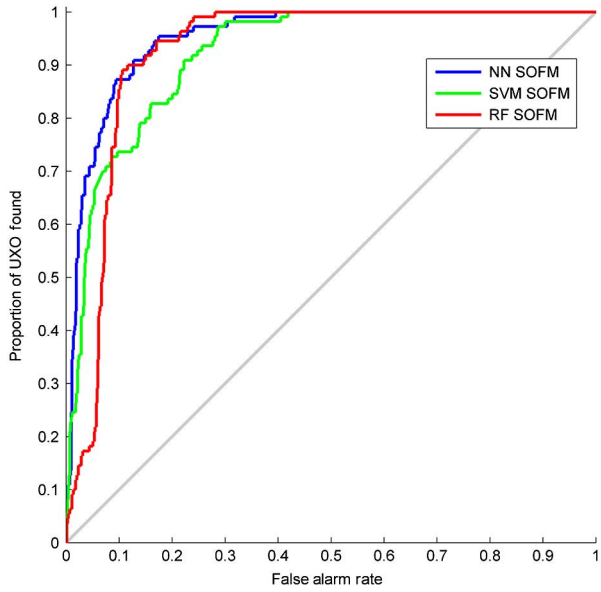

Fig. 8. SOFM preclassification ROC curves for NN, SVM, and RF. RF performed the best with a 100% confidence level at 28%.

TABLE IV
SOFM PRECLASSIFICATION RESULTS FOR LEARNING MACHINES

Learning machine	Confidence level	Centered FAR (%)
NN	90	13
NN	100	39
SVM	90	22
SVM	100	41
RF	90	12
RF	100	28

were used (Table IV). For all UXO to be dug, RF achieved the best results at a FAR of approximately 28% resulting in 203 of 723 NIO to be excavated.

VII. Conclusion

Learning machines can be effective discrimination tools if site characteristics, such as geology, are taken into consideration when developing training sets for discrimination. Our study focused on centered TFM anomalies for learning machine inputs and class selection techniques designed to decrease FAR. We also examined an FEM library method based upon complex UXO shapes, centering of data before application to machine learning, and the application of multiclass discrimination and classification. Geologic effects and elevation variations were not possible to be taken into account during the FEM modeling process and FEM results suffered. Although FEM results had FAR rates above 70%, FEM classification results possibly demonstrate geologic effects or static errors causing magnetic classification to have limited accuracy when site-dependent characteristics are present. FEM or other physics-modeled library methods for magnetics might have success at UXO sites, where geologic interference and static errors are not present or are taken into account during the modeling process.

Gradient centering of anomalies illustrates the importance of correctly positioning TFM anomalies when using learning machines. Centering results decreased all FAR between 21% and 49%, but binary results remained above 40% FAR. To decrease FAR further, SOFM classes were generated for both UXO and NIO separately. SOFM determined classes resulted in a FAR of 28% (RF) and showed FAR can be lowered by creating separate classes when UXO and NIO moments and angles overlap. Using SOFM determined classes helped learning machines decrease FAR by refining distinctions between UXO and NIO anomalies. Our learning machine investigation using FEM targets and real targets from Limestone Hills demonstrate the potential of RF for the discrimination of UXO and NIO, especially using an SOFM preclassification approach.

RF generated the lowest FAR overall and is recommended for future UXO discrimination studies. Although RF was the optimum classifier for Limestone Hills, a thorough comparison of each learning machine is recommended before field implementation. Billings and Youmans [21] stress constant feedback and performance monitoring for "Total Quality Management" of UXO sites. Future studies should focus on separate learning machine implementations for discrimination and classification using both library methods and measured results. Though our FEM library method had high FAR, FEM modeling might be improved by including geologic parameters and varying sensor elevations (as a noise effect) to account for static errors. Finally, future work should examine discrimination employing both TEM and magnetics data.

Acknowledgment

The authors would like to thank the Montana Army National Guard for the Limestone Hills Training Area dataset, the editor, and the anonymous reviewers for their insightful comments.

References

[1] D. W. Butler, P. J. Wolfe, and R. O. Hansen, "Analytical modeling of magnetic and gravity signatures of unexploded ordnance," *J. Environ. Eng. Geophys.*, vol. 6, no. 1, pp. 33–46, Mar. 2001.

[2] S. D. Billings *et al.*, "Unexploded ordnance discrimination using magnetic and electromagnetic sensors: Case study from a former military site," *Geophysics*, vol. 75, no. 3, pp. 103–114, 2010.

[3] Barrett *et al.*, "Optimizing UXO risk mitigation through quantified detection depths and targeted site investigations," presented at the Symp. Appl. Geophys. Eng. Environ. Problems, Tucson, AZ, USA, 2012, p. 348.

[4] L. S. Beran and D. W. Oldenburg "Selecting a discrimination algorithm for unexploded ordnance remediation," *IEEE Trans. Geosci. Remote Sens.*, vol. 46, no. 9, pp. 2547–2557, Sep. 2008.

[5] X. Chen *et al.*, "Spheroidal mode approach for the characterization of metallic objects using electromagnetic induction," *IEEE Trans. Geosci. Remote Sens.*, vol. 45, no. 3, pp. 697–706, Mar. 2007.

[6] Y. Zhang, X. Liao, and L. Carin, "Detection of buried targets via active selection of labeled data: Application to sensing subsurface UXO," *IEEE Trans. Geosci. Remote Sens.*, vol. 42, no. 11, pp. 2535–2543, Nov. 2004.

[7] T. W. Altshuler, "Shape and orientation effects on magnetic signature prediction for unexploded ordnance," in *Proc. UXO Forum*, 1996, pp. 282–291.

[8] H. H. Nelson *et al.*, "Magnetic modeling of UXO and UXO-Like targets and comparison with signatures measured by MTADS," in *Proc. UXO Forum*, 1998, pp. 282–291.

[9] K. M. Churchill, C. Link, and C. C. Youmans, "A comparison of the finite-element method and analytical method for modeling unexploded ordnance using magnetometry," *IEEE Trans. Geosci. Remote Sens.*, vol. 50, no. 7, pp. 2720–2732, Jul. 2012.

[10] S. J. Hart, R. E. Shaffer, S. L. Rose-Pehrsson, and J. R. McDonald, "Using physics-based modeler outputs to train probabilistic neural networks for unexploded ordnance (UXO) classification in magnetometry surveys," *IEEE Trans. Geosci. Remote Sens.*, vol. 39, no. 4, pp. 797–804, Apr. 2001.

[11] H. H. Nelson, T. H. Bell, J. R. McDonald, and B. Barrow, "Advanced MTADS classification for detection and discrimination of UXO," Naval Research Lab., Washington, DC, USA, Tech. Rep. A629904, 2003.

[12] Montana Army National Guard Fort Harrison, Butte Field Office, *Limestone Hills Training Area Land Withdrawal: Final Legislative Environmental Impact Statement*, Apr. 2008.

[13] B. Zhang, K. O'Neill, J. Kong, and T. Grzegorczyk, "Support vector machine and neural network classification of metallic objects using coefficients of the spheroidal mqs response modes," *IEEE Trans. Geosci. Remote Sens.*, vol. 46, no. 1, pp. 159–171, Jan. 2008.

[14] L. S. Beran *et al.*, "Practical strategies for classification of unexploded ordnance," *Geophysics*, vol. 78, no. 1, pp. E41–E46, 2013.

[15] J. R. Wait, "A conducting sphere in a time-varying magnetic field," *Geophysics*, vol. 16, pp. 666–672, 1951.

[16] V. Sanchez, Y. Li, M. N. Nabighian, and D. L. Wright, "Numerical modeling of higher order magnetic moments in UXO discrimination," *IEEE Trans. Geosci. Remote Sens.*, vol. 46, no. 9, pp. 2568–2583, Sep. 2008.

[17] F. Shubitidze, K. O'Neill, K. Sun, and K. Paulsen, "Investigation of broadband electromagnetic induction scattering by highly conducting, permeable, arbitrarily shaped 3-D objects," *IEEE Trans. Geosci. Remote Sens.*, vol. 42, no. 3, pp. 928–942, Mar. 2004.

[18] S. V. Chilaka, D. L. Faircloth, L. S. Riggs, and H. H. Nelson, "Enhanced discrimination among UXO-like targets using extremely low-frequency magnetic fields," *IEEE Trans. Geosci. Remote Sens.*, vol. 44, no. 1, pp. 10–21, Jan. 2006.

[19] COMSOL Multiphysics, *AC/DC Module: User's Guide Version 4.3*. Stockholm, Sweden: COMSOL AB, 2013.

[20] S. D. Billings, C. Pasion, S. Walker, and L. Beran, "Magnetic models of unexploded ordnance," *IEEE Trans. Geosci. Remote Sens.*, vol. 44, no. 8, pp. 2115–2124, Aug. 2006.

[21] S. Billings and C. Youmans, "Experiences with unexploded ordnance discrimination using magnetometry at a live-site in Montana," *J. Appl. Geophys.*, vol. 61, no. 3/4, pp. 194–205, Mar. 2007.

[22] L. Beran, S. Billings, and D. Oldenburg, "Incorporating uncertainty in unexploded ordnance discrimination," *IEEE Trans. Geosci. Remote Sens.*, vol. 49, no. 8, pp. 3071–3080, Aug. 2011.

[23] O. Maimon and L. Rokach, *The Data Mining and Knowledge Discovery Handbook*, 1st ed. New York, NY, USA: Springer, 2005.

[24] S. Varma and R. Simon, "Bias in error estimation when using cross validation for model selection," *BMC Bioinformat.*, vol. 7, p. 91, 2006.

[25] M. T. Hagan, H. B. Demuth, and M. Beale, *Neural Network Design*. Boston, MA, USA: PWS, 1996.

[26] V. Vapnik, *Statistical Learning Theory*. Hoboken, NJ, USA: Wiley, 1998.

[27] J. Weston and C. Watkins, "Multi-class support vector machines," Royal Holloway, Univ. London, London, U.K., Tech. Rep. CSD-TR-98-04, 1998.

[28] S. Canu, Y. Grandvalet, and A. Rakotomamonjy, "SVM and kernel methods Matlab toolbox," in *Perception Systèmes et Information*. Rouen, France: INSA de Rouen, 2003.
[29] L. Breiman, "Random forests," *Mach. Learn.*, vol. 45, no. 1, pp. 5–32, Oct. 2001.
[30] L. Breiman, J. Friedman, R. Olshen, and C. Stone, *Classification of Regression Trees*. Belmont, CA, USA: Wadsworth, 1984.
[31] L. Breiman, "Bagging predictors," *Mach. Learn.*, vol. 24, pp. 123–140, 1996.
[32] R. Daz-Uriarte and S. A. de Andrs, "Gene selection and classification of microarray data using random forest," *BMC Bioinformat.*, vol. 7, no. 1, p. 3, 2006.
[33] G. Izmirlian, "Application of the random forest classification algorithm to a SELDI-TOF proteomics study in the setting of a cancer prevention trial," *Ann. NY Acad. Sci.*, vol. 1020, pp. 154–174, 2004.
[34] A. Liaw and A. Wiener, "Classification and regression by random forest," *R News*, vol. 2, pp. 18–22, 2002.
[35] A. Jaiantilal, "RandomForest-MATLAB: Random forest (regression, classification and clustering) implementation for MATLAB (and standalone)," 2010.
[36] S. D. Billings, "Discrimination and classification of buried unexploded ordnance using magnetometry," *IEEE Trans. Geosci. Remote Sens.*, vol. 42, no. 6, pp. 1241–1251, Jun. 2004.
[37] K. Davis, Y. Li, and M. N. Nabighian, "Automatic detection of UXO magnetic anomalies using extended Euler deconvolution," *Geophysics*, vol. 75, no. 3, pp. G13–G20, May/Jun. 2010.
[38] S. Billings and F. J. Herrmann, "Automatic detection of position and depth of potential UXO using continuous wavelet transforms," in *Proc. AeroSense Int. Soc. Opt. Photon.*, Sep. 2003, pp.1012–1022.
[39] T. Kohonen, "The self-organizing map," *Neurocomputing*, vol. 21, no. 1–3, pp. 1–6, 1998.
[40] T. Kohonen, *Self-Organizing Maps*. 3rd ed. Berlin, Germany: Springer-Verlag, 2001.

Matthew P. Bray received the B.S. degree in geophysical engineering in 2011 and the M.S. degree in geoscience (geophysical engineering option) from Montana Tech, Butte, MT, USA, in 2013. He is currently pursuing a Ph.D. degree in geophysics at Colorado School of Mines with the Reservoir Characterization Project.

During the M.S. degree at Montana Tech, he worked as a Geophysicist with Chevron Corporation, Houston, TX, USA, Apache Oil Corporation, Midland, TX, USA, and Newmont Mining Corporation, Englewood, CO, USA.

Mr. Bray is a member of the Society of Exploration Geophysics, American Association of Petroleum Geologists, Society of Petroleum Engineers, and Environmental and Engineering Geophysical Society.

Curtis A. Link (M'10) received the B.A. degree in physics from the University of Iowa, Iowa City, IA, USA, in 1971, the B.S. degree in geophysical engineering from Montana Tech, Butte, MT, USA, in 1985, and the Ph.D. degree in geophysics from the University of Houston, Houston, TX, USA, in 1993. While in Houston, he did his graduate work in crosswell tomography at the University of Houston's Allied Geophysical Laboratories.

After graduating from Montana Tech, he spent three years in Asia doing land and marine seismic data acquisition and processing for Geophysical Services, Inc. and subsequently Halliburton Geophysical Services (HGS). He was then transferred to the HGS office in Houston, TX, USA, where he worked on processing 3-D seismic data from the North Slope, AK, USA. From 1994 to 2013, he was a Faculty Member of the Geophysical Engineering Department, Montana Tech, where he is currently Professor Emeritus. Since 2014, he is the Director of Freshman Engineering Program, Montana Tech. His research interests include neural network applications in reservoir characterization, unexploded ordnance, and land streamer applications for shallow investigations.

Dr. Link is a member of the Society of Exploration Geophysics, European Association of Geoscientists and Engineers, Environmental and Engineering Geophysical Society, American Geophysical Union, and American Association of Petroleum Geologists.